Synthesis and Electrochemistry of (μ-Oxo)technetium Complexes with Bipyridine and Halide Ligands. Crystal Structures of (μ-O)[X(bpy)$_2$Tc]$_2$X$_2$·bpy (X = Cl, Br) and (μ-O)[Cl(phen)$_2$Tc]$_2$Cl$_2$

Jun Lu, C. D. Hiller, and M. J. Clarke*

Merkert Chemistry Center, Boston College, Chestnut Hill, Massachusetts 02167

Received May 29, 1991

Dinuclear μ-oxo complexes of technetium, in which the two Tc atoms are in intimate electronic communication, have been synthesized and structurally characterized. (μ-O)[X(bpy)$_2$Tc]$_2$X$_2$·bpy, where X = Cl (I) and Br (II), are isomorphic and crystallize in the orthorhombic space group *Pbcn* with the following unit cell parameters: a = 18.29 (1) Å, b = 9.763 (2) Å, c = 25.99 (2) Å, Z = 4, and R = 0.071, for X = Cl, and a = 18.584 (6) Å, b = 9.9602 (8) Å, c = 26.131 (2) Å, Z = 4, and R = 0.032 for X = Br. The compound (μ-O)[Cl(phen)$_2$Tc]Cl$_2$·4H$_2$O (III) also crystallized in *Pbcn* with the following unit cell parameters: a = 17.31 (2) Å, b = 10.61 (2) Å, c = 25.77 (2) Å, Z = 4, and R = 0.075. In each structure, the geometry is distorted octahedral around each Tc, with the equatorial ligands on the opposite metal atoms being staggered relative to one another. The bridging oxygen atom sits on a 2-fold symmetry element which bisects the angle formed by the staggered Tc–X bonds. The molecules are bent along the Tc–O–Tc axes by 171.9(8), 173.0(3), and 171.6(9)°, and the Tc–O bond lengths are 1.824(2), 1.8278(6), and 1.819(3) Å for I, II, and III, respectively. The average equatorial Tc–N bond distance for the three structures is 2.11(2) Å, and the average Tc–N trans to the bridging oxygen is 2.135(22) Å. The Tc–X bond distances are 2.418(4), 2.5665(7), and 2.408(6) Å, for I, II, and III, respectively. Infrared Tc–O stretching frequencies are in the range 723–730 cm^{-1}. Halides are easily dissociated from the phenanthroline complexes and an analog, (μ-O)[(OH)(phen)$_2$Tc]$_2$(PF$_6$)$_2$·6H$_2$O, of a ruthenium water oxidation catalyst has been investigated. Cyclic voltammetry revealed three one-electron couples that are independent of pH over a wide range. At low pH, oxidation of (μ-O)[(OH)(phen)$_2$Tc]$_2^{2+}$ by O$_2$ occurs slowly, but is rapid with HNO$_3$ or H$_2$O$_2$ to give the (III–IV) mixed-valent complex, which exhibits a low energy ("IVCT") band at 959 nm. The comproportionation constant for (μ-O)[(OH)(phen)$_2$Tc]$_2^{2+}$ + (μ-O)[(OH)(phen)$_2$Tc]$_2^{4+}$ → (μ-O)[(OH)(phen)$_2$Tc]$_2^{3+}$ is 3.07 × 10^{10}, consistent with close electronic communication between the two technetium atoms.

Oxo-bridged complexes of mid-transition metals frequently exhibit high thermodynamic stability and, consequently, often emerge as side products in synthetic reactions. Hallmarks of the chemistry of technetium are the prevalence of oxo ions in aqueous solution and the extraordinary stability of TcO$_2$·nH$_2$O.[1,2] Aside from the intrinsic interest in studying strong electronic coupling between electron-transfer centers, μ-oxo complexes also serve as catalysts for water oxidation[3] and, more recently, have been recognized as inhibitors of calcium ion transport in vivo.[4] When [OCl$_4$Tc]$^-$ reacts with neat pyridine derivatives or with these ligands dissolved in noncoordinating organic solvents, a mixture of μ-oxo, mixed-valent complexes eventually results. The first to form is asymmetric, [Cl$_2$(py)$_3$Tc–O–TcCl$_3$(py)$_2$], while a more symmetric species, [Cl(py)$_4$Tc–O–Tc(py)Cl$_4$]· develops later. The two complexes are interconvertable and eventually reach an equilibrium.[5,6]

We have now carried out the parallel reaction with chelating bipyridine and phenanthroline ligands in a poorly coordinating solvent. Steric considerations cause the position cis rather than trans to the μ-oxo to be occupied by the halide ligand. Electronic factors stabilize the [Tc^{III}–Tc^{III}] dimer, which has also been characterized by Breikss and Davison,[7] rather than a mixed-valent species. The structures of (μ-O)[Cl(bpy)$_2$Tc]$_2$Cl$_2$·bpy (I), (μ-O)[Br(bpy)$_2$Tc]$_2$Br$_2$·bpy (II), and (μ-O)[Cl(phen)$_2$Tc]$_2$Cl$_2$·4H$_2$O (III) have been determined. The synthetic method is somewhat more facile than that of Breikss,[7] while still giving high yields. The substitution lability of the halide ligands has also been explored and used to prepare, (μ-O)[(OH)(phen)$_2$Tc]$_2^{2+}$, a close analog of the ruthenium water-oxidation catalyst, which is easily oxidized to a mixed-valent complex. Structural, electronic, and electrochemical comparisons are made between these complexes and the ruthenium water-oxidation catalyst, which explain significant differences in their chemistries.

Experimental Section

Caution! All syntheses were performed with ^{99}Tc, which is a β-emitting isotope with a half-life of 2.15 × 10^5 years. (Only milligram quantities should be handled with the minimum shielding present under normal laboratory conditions.)

Synthesis. The starting materials, [(n-Bu)$_4$N][TcOX$_4$], were prepared from (NH$_4$)TcO$_4$ (Oak Ridge) by the method of Cotton (X = Cl)[8] and by a modification of the method of Preetz (X = Br).[9,10]

The compound, (μ-O)[Br(bpy)$_2$Tc]$_2$Br$_2$·bpy, was prepared by dispersing 200 mg of [(n-Bu)$_4$N][TcOBr$_4$] with 600 mg of 2,2′-bipyridine in 5 mL of DMF. After the mixture was refluxed for 6–8 h, purple crystals were collected by filtration, washed with acetone and diethyl ether, and dried in a vacuum desiccator. Yield: 80%. Anal. Calcd for H$_{40}$C$_{50}$N$_{10}$OBr$_4$Tc$_2$: C, 45.69; H, 3.07; N, 10.66. Found: C, 44.60; H, 3.04; N, 10.44. IR in KBr pellet (cm^{-1}): $\nu_{Tc-O-Tc}$ = 730 (s); 1660 (s), 1602 (s), 1581 (m), 1560 (m) 1445 (vs), 1417 (m), 1314 (s), 1271 (m), 1243 (m), 1152 (m), 1018 (m), 871 (s), 779 (vs), 653 (m). UV–vis in methanol, (λ_{max}, nm) (ϵ, M^{-1} cm^{-1}): 224 (6.79 × 10^4), 290 (5.63 × 10^4),

(1) Clarke, M. J.; Podbielski, L. *Coord. Chem. Rev.* **1987**, *78*, 253–331.
(2) Davison, A.; Jones, A. G. *Int. J. Appl. Radiat. Isot.* **1982**, *33*, 793–99.
(3) Geselowitz, D.; Meyer, T. *Inorg. Chem.* **1990**, *29*, 3894–96.
(4) Ying, W.-L.; Emerson, J.; Clarke, M. J.; Sanadi, D. R. *Biochemistry* **1991**, *30*, 4949–4952.
(5) Clarke, M. J.; Kastner, M. E.; Podbielski, L. A.; Fackler, P. H.; Schreifels, J.; Meinken, G.; Srivastava, S. C. *J. Am. Chem. Soc.* **1988**, *110*, 1818–1827.
(6) Lu, J.; Clarke, M. J. *Inorg. Chem.* **1988**, *27*, 4761–4766.
(7) (7)Breikss, A. I. Ph.D. Thesis, Massachusetts Institute of Technology, 1989.
(8) Cotton, F. A.; Davison, A.; Day, V. W.; Gage, L. D.; Trop, H. S. *Inorg. Chem.* **1979**, *18*, 3024.
(9) Preetz, W.; Peters, G. *Z. Naturforsch.* **1980**, *35B*, 1355–1358.
(10) Kastner, M. E.; Fackler, P. H.; Charkoudian, J.; Podbielski, L.; Charkoudian, J.; Clarke, M. J. *Inorg. Chim. Acta* **1986**, *114*, L11–L15.

0020-1669/93/1332-1417$04.00/0

Table I. Crystallographic Data for $(\mu\text{-O})[Cl(bpy)_2Tc]_2Cl_2\cdot bpy$ (I), $(\mu\text{-O})[Br(bpy)_2Tc]_2Br_2\cdot bpy$ (II), and $(\mu\text{-O})[Cl(phen)_2Tc]_2Cl_2\cdot 4H_2O$ (III)[a,c]

	I	II	III
formula	$Tc_2C_{50}H_{40}N_{10}OCl_4$	$Tc_2C_{50}H_{40}N_{10}OBr_4$	$Tc_2C_{48}H_{36}N_8O_5Cl_4$
fw	1136.56	1314.36	1144.49
space group; crystal syst	*Pbcn* (No. 60); orthorhombic	*Pbcn* (No. 60); orthorhombic	*Pbcn* (No. 60); orthorhombic
cell constants (Å)			
a	18.29(1)	18.584(6)	17.31(3)
b	9.763(2)	9.9602(8)	10.61(2)
c	25.99(2)	26.131(2)	25.77(2)
cell volume (Å^3)	4642(7)	4837(3)	4735(18)
Z (fw/unit cell)	4	4	4
T (°C)	22(1)	22(1)	22(1)
radiation source (graphite monochromated)	Cu Kα (λ = 1.541 78 Å)	Cu Kα (λ = 1.541 78 Å)	Cu Kα (λ = 1.541 78 Å)
d_{calcd} (g/cm^3)	1.621	1.80	1.606
μ (cm^{-1})	74.03	89.42	73.15
rel. transm factors	0.62–1.0	0.76–1.0	0.85–1.0
$R = \sum(\|F_o\| - \|F_c\|)/\sum\|F_o\|$	0.071	0.032	0.075
$R_w = [\sum w(\|F_o\| - \|F_c\|)^2/\sum w\|F_o\|^2]^{1/2}$ [b]	0.092	0.045	0.086

[a] Reflections with $I > 3\sigma(I)$ were retained as observed and used in the solution and refinement of the structure. Three standard reflections were monitored with a limit of 0.2% variation. Function minimized $\sum w(|F_o| - |F_c|)^2$. [b] Weighting scheme: $w = 4F_o^2/\sigma^2(F_o)^2$. [c] All calculations were performed by using the TEXSAN–TEXRAY Structure Analysis Package, Molecular Structure Corp., 1985.

Table II. Positions for the Non-Hydrogen Atoms in $(\mu\text{-O})[Cl(bpy)_2Tc]_2\cdot bpy$ (I) and $(\mu\text{-O})[Br(bpy)_2Tc]_2Br_2\cdot bpy$ (II)

atom	*x*	*y*	*z*	*B*(eq)	*x*	*y*	*z*	*B*(eq)
Tc1	0.58307(6)	0.1028(1)	0.71151(4)	3.24(5)	0.08170(2)	0.09076(4)	0.21130(1)	2.18(2)
X1	0.6371(2)	0.3214(4)	0.7330(1)	4.7(2)	0.13830(3)	0.31835(6)	0.23369(2)	3.66(3)
X2	0.1560(2)	0.1156(5)	0.5524(2)	6.1(2)	0.65466(3)	0.10835(7)	0.05231(2)	4.31(3)
O	1/2	0.116(1)	3/4	3.9(6)	0	0.1020(4)	1/4	2.2(2)
N1	0.6433(6)	–0.005(1)	0.7699(4)	4.1(6)	0.1401(2)	–0.0173(4)	0.2682(1)	2.6(2)
N2	0.5596(6)	–0.105(1)	0.6933(4)	3.9(6)	0.0570(2)	–0.1104(4)	0.1925(2)	2.5(2)
N3	0.5354(6)	0.203(1)	0.6488(4)	4.2(6)	0.0363(2)	0.1896(4)	0.1485(1)	2.6(2)
N4	0.6640(6)	0.083(1)	0.6526(4)	3.7(5)	0.1622(2)	0.0728(4)	0.1524(2)	2.7(2)
N5	0.415(1)	–0.009(3)	0.5383(7)	11(1)	0.0872(4)	–0.0036(8)	0.4636(3)	8.5(5)
C1	0.6833(8)	0.052(2)	0.8048(5)	4.5(8)	0.1817(3)	0.0345(6)	0.3039(2)	3.5(3)
C2	0.7167(9)	–0.028(2)	0.8435(6)	6(1)	0.2155(3)	–0.0410(7)	0.3409(2)	4.2(3)
C3	0.705(1)	–0.166(2)	0.8462(7)	6(1)	0.2054(3)	–0.1763(7)	0.3406(2)	4.5(3)
C4	0.663(1)	–0.222(2)	0.8083(7)	6(1)	0.1645(3)	–0.2337(6)	0.3033(2)	4.1(3)
C5	0.6336(7)	–0.145(2)	0.7682(6)	4.1(7)	0.1321(3)	–0.1529(6)	0.2657(2)	3.2(3)
C6	0.5902(8)	–0.198(1)	0.7260(5)	3.8(7)	0.0889(3)	–0.2036(6)	0.2234(2)	3.3(3)
C7	0.580(1)	–0.338(2)	0.7167(8)	8(1)	0.0789(4)	–0.3388(6)	0.2142(3)	5.0(4)
C8	0.540(1)	–0.372(2)	0.6710(9)	7(1)	0.0373(4)	–0.3771(7)	0.1726(3)	5.7(4)
C9	0.508(1)	–0.281(2)	0.6431(6)	5(1)	0.0050(3)	–0.2816(7)	0.1426(2)	4.8(3)
C10	0.5201(8)	–0.147(2)	0.6536(6)	4.4(8)	0.0176(3)	–0.1485(6)	0.1536(2)	3.6(3)
C11	0.4707(7)	0.264(2)	0.6493(5)	4.1(7)	0.0282(3)	0.2534(6)	0.1500(2)	3.2(2)
C12	0.4448(9)	0.344(2)	0.6102(6)	4.8(8)	0.0515(3)	0.3332(6)	0.1103(2)	3.8(3)
C13	0.489(1)	0.364(2)	0.5672(6)	6(1)	0.0091(4)	0.3502(6)	0.0684(2)	4.3(3)
C14	0.5564(8)	0.295(2)	0.5629(6)	4.8(8)	0.0565(3)	0.2881(6)	0.0661(2)	4.0(3)
C15	0.5797(9)	0.214(2)	0.6050(5)	4.4(8)	0.0777(3)	0.2064(5)	0.1062(2)	2.8(2)
C16	0.6498(7)	0.144(1)	0.6071(5)	3.9(7)	0.1472(3)	0.1338(5)	0.1080(2)	2.9(2)
C17	0.6936(9)	0.126(2)	0.5653(6)	5.4(9)	0.1929(3)	0.1261(6)	0.0663(2)	4.1(3)
C18	0.757(1)	0.057(2)	0.5691(6)	7(1)	0.2563(3)	0.0491(7)	0.0715(2)	4.8(3)
C19	0.7751(8)	–0.007(2)	0.6169(7)	6(1)	0.2713(3)	–0.0094(7)	0.1171(2)	4.5(3)
C20	0.7272(8)	0.015(2)	0.6585(6)	4.8(8)	0.2240(3)	0.0033(6)	0.1565(2)	3.6(3)
C21	0.343(1)	0.087(4)	0.531(1)	16(3)	0.0343(3)	0.0379(7)	0.4991(2)	4.5(3)
C22	0.323(3)	0.215(5)	0.514(2)	32(5)	0.0439(3)	0.1376(6)	0.5312(2)	4.4(3)
C23	0.392(1)	0.217(3)	0.467(1)	11(2)	0.1026(4)	0.2063(8)	0.5298(3)	6.7(4)
C24	0.456(1)	0.138(2)	0.4680(7)	7(1)	0.1584(4)	0.182(1)	0.4960(3)	7.2(5)
C25	0.465(1)	0.032(2)	0.5027(7)	6(1)	0.1505(4)	0.074(1)	0.4634(3)	6.8(5)

322 (5.2 × 10^4), 532 (1.82 × 10^4). When the compound was recrystallized from methanol, elemental analyses indicated that the intercalated bipyridine was replaced by water.

$(\mu\text{-O})[Cl(bpy)_2Tc]_2Cl_2\cdot bpy$ was similarly prepared. Anal. Calcd for $H_{40}C_{50}N_{10}OCl_4Tc_2$: C, 52.84; H, 3.55; N, 12.32. Found: C, 52.29; H, 3.49; N, 12.37. IR in KBr pellet (cm^{-1}): $\nu_{Tc\text{-}O\text{-}Tc}$ = 730 (s); 1637 (m), 1602 (s), 1560 (s), 1468 (m), 1445 (s), 1426 (m), 1314 (m), 1271 (m), 1159 (m), 1025 (m), 878 (s), 772 (vs). UV–vis in methanol, (λ_{max}, nm) (ϵ, M^{-1} cm^{-1}): 219 (7.1 × 10^4), 289 (6.1 × 10^4), 322 (sh), 531 (1.78 × 10^4). The ^{1}H NMR was identical to that reported by Breikss.[7] Recrystalization from methanol resulted in loss of the intercalated bipyridine, which was replaced with varying amounts of water. Anal. Calcd for $H_{32}C_{40}N_8OCl_4Tc_2\cdot 7H_2O$: C, 43.42; H, 4.19; N, 10.13; Cl, 12.82. Found: C, 43.82; H, 4.14; N, 10.05; Cl, 12.53.

While $(\mu\text{-O})[Cl(phen)_2Tc]_2Cl_2\cdot 9H_2O$ was similarly prepared with *o*-phenanthroline as the ligand, single crystals of $(\mu\text{-O})[Cl(phen)_2Tc]_2Cl_2\cdot 4H_2O$ were obtained by allowing acetone to vapor diffuse into an ethanol solution of the nonahydrate. Anal. Calcd for $H_{32}C_{48}N_8OCl_4Tc_2\cdot 9H_2O$: C, 46.55; H, 4.07; N, 9.05; Cl, 11.45; Tc, 15.97. Found: C, 46.54; H, 4.05; N, 9.07. IR in KBr pellet (cm^{-1}): $\nu_{Tc\text{-}O\text{-}Tc}$ = 723 (s); 1623 (s), 1602 (m), 1581 (m), 1510 (m), 1426 (s), 1412 (m), 1340 (m), 1252 (m), 1222 (m), 1145 (m), 1103 (m), 920 (s), 899 (s), 850 (vs), 786 (m), 653 (m). UV–vis in methanol, (λ_{max}, nm) (ϵ, M^{-1} cm^{-1}): 289 (8.6 × 10^4), 360 (sh), 526 (2.04 × 10^4).

$(\mu\text{-O})[(OH)(phen)_2Tc]_2(PF_6)_2\cdot 6H_2O$ was prepared by dissolving 100 mg of $(\mu\text{-O})[Cl(phen)_2Tc]_2Cl_2\cdot 9H_2O$ in a minimum amount of water and loading the solution onto a Sephadex CM-25 ion exchange column. The band containing the dihydroxo complex eluted in 0.2 M sodium carbonate at pH 12–13. After rotary evaporation to dryness, the residue was dissolved in 20 mL absolute ethanol, filtered, rotary evaporated again, and dissolved in a minimum volume of water. A few drops of saturated NH_4PF_6 were added to induce precipitation. Anal. Calcd for $H_{34}C_{48}N_8O_3P_2F_{12}Tc_2\cdot 6H_2O$: C, 42.18; H, 3.39; N, 8.20. Found: C, 42.55; H, 3.31; N, 7.69. Chloride analysis was negative. IR in KBr pellet (cm^{-1}): $\nu_{Tc\text{-}O\text{-}Tc}$ = 723 (s); 1630 (m), 1609 (m), 1581 (w), 1412 (w), 1342 (w), 1256 (w), 1222(w), 1145 (w), 843 (vs), 561 (s). UV–vis in

Table III. Positions for the Non-Hydrogen Atoms in (μ-O)[Cl(phen)$_2$Tc]$_2$Cl$_2$·4H$_2$O (III)

atom	x	y	z	B(eq)
Tc	0.9120(1)	0.2120(1)	0.21179(6)	4.97(7)
Cl1	0.8457(3)	0.0284(4)	0.2438(2)	6.3(3)
Cl2	0.4249(5)	0.1925(6)	0.5278(2)	11.2(5)
O	1.0000	0.199(1)	1/4	6(1)
O1	0.605(1)	0.103(2)	0.4984(7)	13(1)
O2	0.260(2)	0.190(2)	0.0625(6)	19(2)
N1	0.863(1)	0.334(1)	0.2683(5)	4.8(8)
N2	0.9431(8)	0.390(1)	0.1821(6)	5.1(8)
N3	0.954(1)	0.100(1)	0.1503(6)	5.3(9)
N4	0.822(1)	0.228(1)	0.1568(6)	5.6(9)
C1	0.826(1)	0.306(2)	0.3110(8)	7(1)
C2	0.801(1)	0.397(2)	0.3463(8)	7(1)
C3	0.814(1)	0.519(2)	0.3367(9)	8(1)
C4	0.853(1)	0.558(2)	0.2897(8)	6(1)
C5	0.868(2)	0.686(2)	0.275(1)	8(1)
C6	0.906(2)	0.712(2)	0.233(1)	7(1)
C7	0.932(1)	0.614(2)	0.1982(8)	7(1)
C8	0.971(1)	0.637(2)	0.152(1)	8(1)
C9	0.995(2)	0.538(2)	0.1220(8)	8(1)
C10	0.981(1)	0.415(2)	0.1392(8)	6(1)
C11	0.918(1)	0.491(2)	0.2130(8)	7(1)
C12	0.876(1)	0.458(2)	0.2574(7)	5(1)
C13	1.019(1)	0.042(2)	0.1467(7)	6(1)
C14	1.038(1)	−0.037(2)	0.1061(9)	7(1)
C15	0.989(2)	−0.052(2)	0.0659(8)	6(1)
C16	0.921(1)	0.013(2)	0.0664(7)	5(1)
C17	0.862(2)	0.001(2)	0.0276(9)	7(1)
C18	0.796(2)	0.065(2)	0.0296(8)	7(1)
C19	0.776(1)	0.147(2)	0.0731(8)	6(1)
C20	0.710(2)	0.213(2)	0.0793(8)	7(1)
C21	0.699(1)	0.289(2)	0.122(1)	7(1)
C22	0.757(1)	0.289(2)	0.1597(7)	6(1)
C23	0.834(1)	0.154(2)	0.1127(7)	5(1)
C24	0.903(1)	0.090(2)	0.1091(7)	5(1)

acetonitrile, (λ_{max}, nm) (ϵ, M^{-1} cm^{-1}): 288 (8.45 × 10^4), 360 (sh); 520 (1.9 × 10^4); in water an additional peak occurred at 702 nm (950 M^{-1} cm^{-1}).

(μ-O)[(OH)(phen)$_2$Tc]$_2$(PF$_6$)$_3$·5H$_2$O was prepared by dissolving 10–20 mg of (μ-O)[Cl(phen)$_2$Tc]$_2$Cl$_2$9H$_2$O in 20–40 mL of water and adding concentrated HNO$_3$ dropwise with constant stirring. This first formed a purple precipitate, which redissolved on further addition of HNO$_3$ to yield an orange solution. The final concentration of HNO$_3$ was 0.2–0.8 M. The solution was allowed to stand for 20 min before filtering through filter paper to remove some undissolved orange solid. Following the addition of a concentrated solution of NH$_4$PF$_6$ to the filtrate, a brownish-orange solid was collected by filtration. Anal. Calcd for $H_{34}C_{48}N_8O_3P_3F_{18}Tc_2$·5H$_2$O: C, 38.60; H, 2.97; N, 7.50. Found: C, 38.58; H, 2.58; N, 7.60. Chloride analysis was negative. IR in KBr pellet (cm^{-1}): $\nu_{Tc-O-Tc}$ = 721 (s); 1629 (m), 1609 (m), 1581 (w), 1518 (w), 1409 (w), 1342 (w), 1256 (w), 1220 (w), 1141 (w), 850 (vs), 554 (s). UV–vis–near-IR in water, (λ_{max}, nm) (ϵ, M^{-1} cm^{-1}): 278 (9.0 × 10^4), 407 (sh), 490 (1.5 × 10^4), 959 nm (560) (IVCT).

Compound Characterization. All elemental analyses were performed by the Galbraith Laboratories. Infrared spectra were taken on a Nicolet 510-FTIR spectrophotometer in KBr pellets. UV–vis–near-IR spectra were obtained on a Cary Model 2300 spectrophotometer. Magnetic susceptibility studies were performed on a Cahn Model 7500 Electrobalance equipped with a 14 502-G permanent magnet at room temperature.

Electrochemical measurements were performed in aqueous solution at μ = 0.1 (LiCl or HNO$_3$) or 0.1 M tetraethylammonium perchlorate (TEAP) in acetonitrile on a versatile electrochemical apparatus constructed in this laboratory. A carbon paste or platinum button working electrode, Ag/AgCl reference electrode, and platinum wire auxiliary electrode were used in all measurements. Reduction potentials were determined at the midpoint between the anodic and cathodic peaks of the cyclic voltammetric waveform (scanned at 125 mV/s) or at the peak of the square-wave voltammetric waveform (scanned at 1000 mV/s). Wherever possible, potentials were internally referenced against the ferrocene couple (400 mV vs NHE)[11] in nonaqueous media and the [(NH$_3$)$_6$Ru]$^{3+,2+}$ (57 mV) couple in water. When sample and standard peaks overlapped, external references to the standard couples in the same media were used.

(11) Gagné, R. R.; Koval, C. A.; Lisensky, G. C. *Inorg. Chem.* **1980**, *19*, 2854–2855.

Table IV. Bond Distances (Å) Surrounding the Tc Atom in (μ-O)[Cl(bpy)$_2$Tc]$_2$Cl$_2$·bpy (I), (μ-O)[Br(bpy)$_2$Tc]$_2$Br$_2$·bpy (II), and (μ-O)[Cl(phen)$_2$Tc]$_2$Cl$_2$·4H$_2$O (III)

	I	II	III
Tc–O	1.824(2)	1.8278(6)	1.819(3)
Tc–N1	2.15(1)	2.132(4)	2.12(1)
Tc–N2	2.13(1)	2.114(4)	2.11(1)
Tc–N3	2.09(1)	2.091(4)	2.11(1)
Tc–N4	2.14(1)	2.154(4)	2.11(2)
Tc–Br1		2.5665(7)	
Tc–Cl1	2.418(4)		2.408(6)

Table V. Bond Angles Surrounding the Tc Atom in (μ-O)[Cl(bpy)$_2$Tc]$_2$Cl$_2$·bpy (I), (μ-O)[Br(bpy)$_2$Tc]$_2$Br$_2$·bpy (II), and (μ-O)[Cl(phen)$_2$Tc]$_2$Cl$_2$·4H$_2$O (III)

	I L = bpy X = Cl	II L = bpy X = Br	III L = phen X = Cl
Tc–O–Tc	171.9(8)	173.0(3)	171.6(9)
O–Tc–N1	94.3(4)	93.9(1)	90.4(5)
O–Tc–N2	91.2(5)	90.4(2)	92.8(6)
O–Tc–N3	92.7(4)	94.0(1)	94.3(5)
O–Tc–N4	167.4(3)	167.8(1)	170.7(4)
O–Tc–X	98.7(4)	99.2(1)	98.9(4)
N1–Tc–N2	78.1(5)	78.1(2)	78.6(6)
N1–Tc–N3	173.0(5)	171.9(1)	174.5(6)
N1–Tc–N4	96.1(4)	95.9(1)	96.8(6)
N2–Tc–N3	100.8(5)	100.1(2)	98.2(6)
N2–Tc–N4	83.9(4)	84.6(1)	82.9(6)
N3–Tc–N4	76.9(5)	76.0(2)	78.3(6)
X–Tc–N1	93.4(4)	94.5(1)	94.0(4)
X–Tc–N2	167.5(3)	168.3(1)	166.3(4)
X–Tc–N3	86.5(3)	85.9(1)	88.1(4)
X–Tc–N4	87.9(3)	87.2(1)	86.6(4)

Structure Determinations. Single crystals of (μ-O)[X(bpy)$_2$Tc]$_2$X$_2$·bpy (X = Cl, Br) were mounted on a glass fiber, which were placed in the beam of a Rigaku AFC5R diffractometer. Pertinent crystal data is given in Table I. On the basis of systematic absences of $0kl$, $k \neq 2n$; $h0l$, $l \neq 2n$; and $hk0$, $h + k \neq 2n$ the space group was determined to be *Pbcn*. Intensities of three representative reflections, which were measured after every 150 reflections, remained constant throughout data collection so that no decay correction was necessary; however, an empirical absorption correction was applied. The Tc and the majority of other atoms were located by direct methods and the remaining atoms were found from difference Fourier maps.[12,13] While there is a possible disorder in the N and C placements in the intercalated bpy, an attempt to treat this did not improve the *R* value significantly. A slight rotation about the bridging carbons would account for the relatively high thermal parameters for this group. The non-hydrogen atoms were refined anisotropically. Hydrogen atoms were included in the structure factor calculation in idealized positions (C–H = 0.95 Å, O–H = 0.82 Å) and were assigned isotropic thermal parameters, which were 20% greater than the B_{equiv} value of the atoms to which they were bonded. Refinement was by full-matrix least-squares methods. Neutral atom scattering factors[14] and anomalous dispersion effects were included in F_{calc};[15] the values for $\Delta f'$ and $\Delta f''$ were those of Cromer.[14] All calculations were performed using the TEXSAN–TEXRAY Structure Analysis Package, Molecular Structure Corp., 1985. Table II lists the atomic positions for (μ-O)[X(bpy)$_2$Tc]$_2$X$_2$·bpy, where X = Cl and Br.

The structure of (μ-O)[Cl(phen)$_2$Tc]$_2$Cl$_2$·4H$_2$O was similarly determined. Electron density corresponding to a hydrogen atom was located between O1 and Cl2 on difference maps. H20 was inserted at an idealized position and refined isotropically. Table III lists the atomic positions for this compound.

MO Energy Calculations. ZINDO (INDO/1),[16] IEHT[17] calculations were performed on a CaChe workstation[18] by using the crystallographic coordinates in Table III and ammines as the nitrogen ligands.

(12) Gilmore, C. J. *J. Appl. Crystallogr.* **1984**, *17*, 42–46.
(13) Beurskens, P. T. *DIRDIF. Technical Report*; University of Nijmegen, Crystallographic Laboratory: Nijmegen, The Netherlands, 1984.
(14) Cromer, D. T.; Weber, J. T. In *International Tables for X-ray Crystallography*; Kynoch Press: Birmingham, England, 1974; Vol. IV; pp Tables 2.2A and 2.3.1.
(15) Ibers, J. A.; Hamilton, W. C. *Acta Crystallogr.* **1964**, *17*, 781.

Table VI. Electrochemical Parameters for Technetium Oxidation–Reduction Couples of $(\mu\text{-O})[X(L)_2Tc]_2^{2+}$ [a]

complex	E_1 (V)	E_2 (V)	E_3 (V)	media
$(\mu\text{-O})[Cl(bpy)_2Tc]_2^{2+}$		0.810 ± 0.003	−0.584 ± 0.005	0.1 M LiCl/H_2O
	1.334 ± 0.008	0.666 ± 0.007	−0.733 (irrev, red)	0.1 M TEAP/CH_3CN
			−0.827 (irrev, oxid)	
$(\mu\text{-O})[Br(bpy)_2Tc]_2^{2+}$		0.846 ± 0.009	−0.570 ± 0.08	0.1 M LiCl/H_2O
	1.362 ± 0.002	0.703 ± 0.010	−0.712 (irrev, red)	0.1 M TEAP/CH_3CN
			−0.840 (irrev, oxid)	
$(\mu\text{-O})[Cl(phen)_2Tc]_2^{2+}$		0.814 ± 0.004	−0.505 (irrev, oxid)	0.1 M LiCl/H_2O
			−0.714 (irrev, red)	
	1.315 ± 0.006	0.651 ± 0.002	−0.908 (irrev)	0.1 M TEAP/CH_3CN
$(\mu\text{-O})[(OH)(phen)_2Tc]_2^{2+}$	1.434 ± 0.006[a]	0.814 ± 0.004	−0.676 (irrev, oxid)	a) 0.1 M HNO_3
			−0.891 (irrev, red)	b) 0.1 M $NH_4(HCO_2)$
	1.327 ± 0.006	0.658 ± 0.002	−0.727 (rev 1st scan)	0.1 M TEAP/CH_3CN

[a] Reduction potentials are assigned as follows:

$$Tc^{IV}\text{–O–}Tc^{IV} \xrightarrow{E_1} Tc^{IV}\text{–O–}Tc^{III} \xrightarrow{E_2} Tc^{III}\text{–O–}Tc^{III} \xrightarrow{E_3} Tc^{III}\text{–O–}Tc^{II}$$

Results

Synthesis. Compounds with the general formulation, $(\mu\text{-O})[XL_2Tc]_2X_2$, where L = bpy or phen and X = Cl, were readily synthesized by refluxing $[(n\text{-}Bu)_4N](TcOX_4)$ and the heterocyclic ligand in DMF. When L = bipyridine, the free ligand co-crystallized from the reaction mixture in a 1:1 ratio with the compound, but was easily replaced by water on recrystalization. Phenanthroline did not co-crystallize, so that III was isolated as a hydrate of four or nine water molecules depending on the precipitation conditions. Magnetic susceptibility measurements determined I, II, and III to be diamagnetic. The chloride ligands are easily lost from the phenanthroline complex and could be removed completely by chromatography on a cation-exchange column. On the other hand, the hydroxide analogs of the bipyridine complexes could not be easily isolated.

When solutions of $(\mu\text{-O})[(OH)(phen)_2Tc]_2Cl_2\cdot 6H_2O$ were acidified with concentrated HNO_3, a purple solid precipitated, which dissolved to yield an orange solution upon further addition of acid. Similar results could be obtained more directly by adjusting solutions of $(\mu\text{-O})[Cl(phen)_2Tc]_2Cl_2\cdot 9H_2O$ to pH ~0.5 with HNO_3. Solutions of the orange material in 0.05 M nitric acid persisted for weeks. In 1 M HNO_3 or upon addition of Ce^{IV} to these solutions the color gradually changed to yellow and then colorless, with an absorption maximum coincident with that of pertechnetate. Passage of ceric-oxidized solutions through a cation-exchange column, which retained the starting material and partially oxidized products, yielded a solution with the absorption spectrum of $[TcO_4]^-$, which also exhibited HPLC retention times identical to those of $[TcO_4]^-$. Oxidation also occurred in nitric acid solutions that had been thoroughly purged with argon, so that O_2 is not the oxidant. Raising the pH of these orange solutions with argon-purged NaOH quickly restored the purple color.

Addition of other acids (HCl, $HClO_4$, F_3CCSO_3H, etc.) to purple solutions of $(\mu\text{-O})[Cl(phen)_2Tc]_2Cl_2$ yielded a purple precipitate, which only very slowly dissolved to give orange solutions. Addition of Ce^{IV} to the purple, perchloric acid solution of $(\mu\text{-O})[Cl(phen)_2Tc]_2Cl_2$ with its purple precipitate caused the solution to quickly turn orange and gradually oxidized the purple solid to orange. Addition of 5 equiv of H_2O_2 to the purple hydrochloric acid solution (pH < 1) caused rapid oxidation to the orange form, which persisted for hours before gradually turning to a pale yellow. Raising the pH with NaOH caused a rapid return of the purple color. At pH > 2 peroxide would not oxidize the purple compound.

When the brown-orange $(\mu\text{-O})[(OH)(phen)_2Tc]_2(PF_6)_3\cdot 5H_2O$ was dissolved in water, the solution changed to purple over a period of several hours at pH ~2. At pH > 3–4 (adjusted with NaOH) solutions immediately changed to purple, with a purple precipitate occurring in basic media. Precipitation at neutral pH was also noted in relatively concentrated (millimolar) solutions.

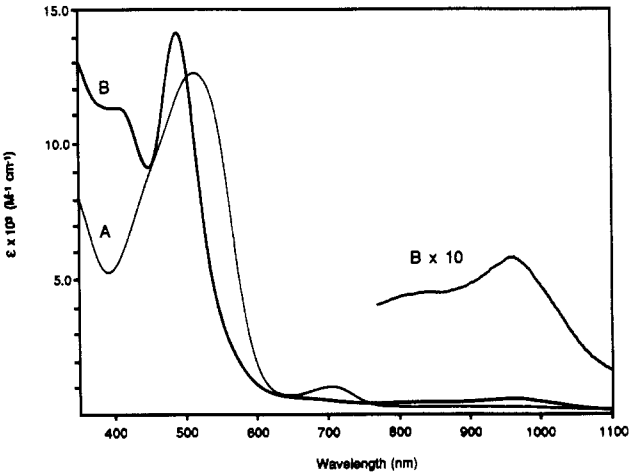

Figure 1. (a) Spectrum of $(\mu\text{-O})[(OH)(phen)_2Tc]_2^{2+}$ in 0.1 M $NaNO_3$, pH 7.1. (b) Spectrum of $(\mu\text{-O})[(OH)(phen)_2Tc]_2^{3+}$ in 0.1 M HNO_3.

Dissolution of $(\mu\text{-O})[(OH)(phen)_2Tc]_2(PF_6)_3\cdot 5H_2O$ in 1 M HCl resulted in orange solutions that were stable to spectral changes for over 1 month, whereas those in 1 M HNO_3 decomposed over several days. When the pH of a solution of $(\mu\text{-O})[(OH)(phen)_2Tc]_2(PF_6)_3$ was raised from 0–7 in nitric acid media by addition of NaOH, isosbestic points occurred at 437 and 478 nm, and λ_{max} shifted from 490 nm at pH 1 to 505 nm at pH 3.5 and finally to 525 nm at pH 5.

Spectra. Complexes of the type $(\mu\text{-O})[XL_2Tc]_2^{2+}$ all absorbed strongly and broadly around 322 nm and 520–530 nm in addition to the π–π^* ligand-centered transitions around 280–290 nm. The complexes exhibited Tc–O–Tc stretching bands at 720–730 cm^{-1}, which is in the range observed for similar $(\mu\text{-O})Tc$ complexes,[10] but somewhat higher in energy than that observed in $(\mu\text{-O})[OM(Et_2dtc)_2]_2$, where Et_2dtc = ethyldithiocarbamate and M = Tc (ν_{MOM} = 630 cm^{-1}) and Re (ν_{MOM} = 665 cm^{-1}).[19] Dissolving $(\mu\text{-O})[(OH)(phen)_2Tc]_2(PF_6)_3$ in acetonitrile or III in 1 M HNO_3 revealed a band at 959 nm. When the mixed-valent complex in acetonitrile was reduced to the purple form with ferrocene, the 959-nm peak disappeared and was not evident in the spectrum of $(\mu\text{-O})[Cl(phen)_2Tc]_2Cl_2$ under the same conditions. The spectra of $(\mu\text{-O})[(OH)(phen)_2Tc]_2^{2+}$ and the mixed-valent complex, $(\mu\text{-O})[(OH)(phen)_2Tc]_2^{3+}$, in aqueous solution are shown in Figure 1.

Electrochemistry. Formal reduction potentials as determined by cyclic and square-wave voltammetry in both water and acetonitrile are in Table VI. Absent from the table are listings

(16) Anderson, W. P.; Cundarai, T. R.; Drago, R. S.; Zerner, M. C. *Inorg. Chem.* **1990**, *29*, 1.
(17) Hoffmann, R. *J. Chem. Phys.* **1963**, *39*, 1397.
(18) CAChe, ZINDO, 2.7, 1991, CAChe Scientific, Inc., Beaverton, OR.
(19) Trop, H. S. Ph.D. Thesis, Massachusetts Institute Technology, 1979.

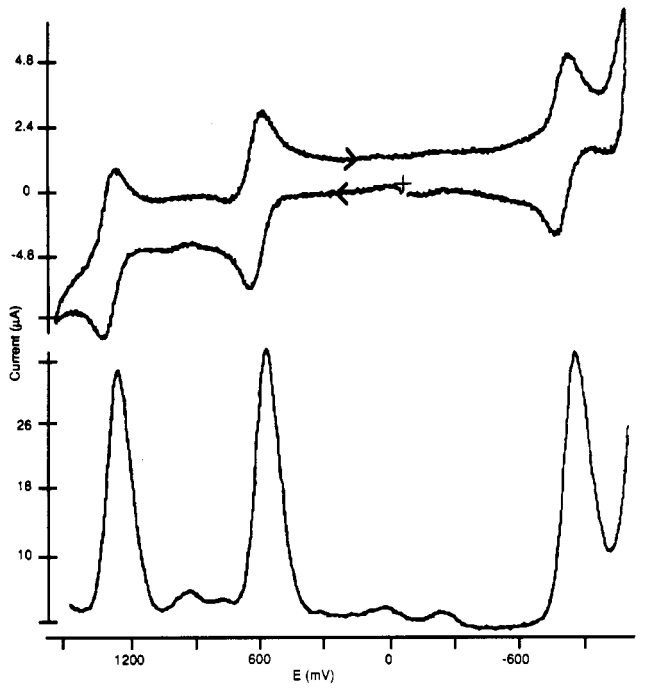

Figure 2. (a) Cyclic voltammogram of $(\mu\text{-O})[HO(phen)_2Tc]_2^{2+}$ in 0.1 M TEAP in argon-purged acetonitrile with a Pt working electrode and potentials relative to Ag/AgCl. Scan rate 125 mV/s. Compound concentration is 2 mM. (b) Square-wave voltammogram of same solution as in part a. Scan rate = 1000 mV/s. Reduction potentials are assigned as $Tc^{IV}\text{–O–}Tc^{IV} \xrightarrow{E_1} Tc^{IV}\text{–O–}Tc^{III} \xrightarrow{E_2} Tc^{III}\text{–O–}Tc^{III} \xrightarrow{E_3} Tc^{III}\text{–O–}Tc^{II}$.

of the irreversible oxidations of the halide counter ions in acetonitrile, which occurred at approximately 1.03 V for chloride and 0.77 V for bromide. Figure 2 shows cyclic and square-wave voltammograms of $(\mu\text{-O})[(HO)(phen)_2Tc]_2^{2+}$ in acetonitrile. The three reduction processes observed in acetonitrile are assigned as

$$Tc^{IV}\text{–O–}Tc^{IV} \xrightarrow{E_1} Tc^{IV}\text{–O–}Tc^{III} \xrightarrow{E_2}$$

$$Tc^{III}\text{–O–}Tc^{III} \xrightarrow{E_3} Tc^{III}\text{–O–}Tc^{II}$$

which are in keeping with the nature of the metal-centered HOMO's and LUMO's (see below). When an equimolar amount of ferrocene was added to the acetonitrile solutions of the complexes, cyclic wave forms of the same size and shape were obtained for the ferrocene couple, verifying that these are single-electron couples. Subsequent scans on platinum electrodes revealed substantial changes in the waveform for E_3, which shifted cathodically and exhibited an increased reduction current and a decreased oxidation current. Irreversible wave forms were evident on the first scan with carbon paste electrodes.

In dilute aqueous HNO_3 between pH 0.5 and 3.0, the couple corresponding to E_1 for $(\mu\text{-O})[OH(phen)_2Tc]_2^{2+}$ was easily observed. Above this range or in the presence of other oxidizable ions, such as halides, the peak was obscured by background currents. In water, E_2 remained constant for all complexes between pH 0.5 and 12. E_3 was reversible for the bipyridine complexes, but was irreversible for the phenanthroline complexes. In solutions below pH ~4, subsequent scans of I and III revealed two additional, reversible, pH-dependent couples. One is situated between E_1 and E_2 and the second generally appears as a shoulder on the E_2 wave. Both of these increased on repetitive scanning.

Structure Descriptions. The structure of $(\mu\text{-O})[Cl(bpy)_2Tc]_2^{2+}$ is shown in Figure S1, $(\mu\text{-O})[Br(bpy)_2Tc]_2^{2+}$ is illustrated in Figure 3, and $(\mu\text{-O})[Cl(phen)_2Tc]_2^{2+}$ in Figure 4. Reference to the atom position listings in Table I reveals a high degree of isomorphism in the structures of $(\mu\text{-O})[X(bpy)_2Tc]_2X_2\cdot bpy$, where X = Cl and Br. Figure S2 illustrates the packing for $(\mu\text{-O})[Br(bpy)_2Tc]_2Br_2\cdot bpy$, which is essentially identical to that in $(\mu\text{-O})[Cl(bpy)_2Tc]_2Cl_2\cdot bpy$. In both structures, free bipyridine

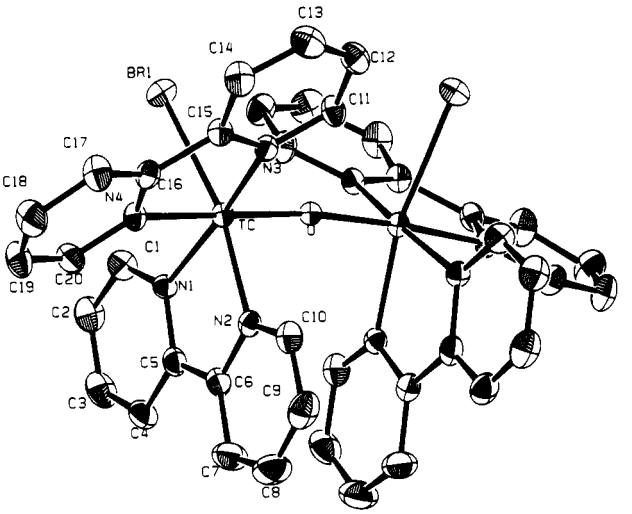

Figure 3. ORTEP diagram of $(\mu\text{-O})[Br(bpy)_2Tc]_2^{2+}$ with thermal ellipsoids at 30% probability.

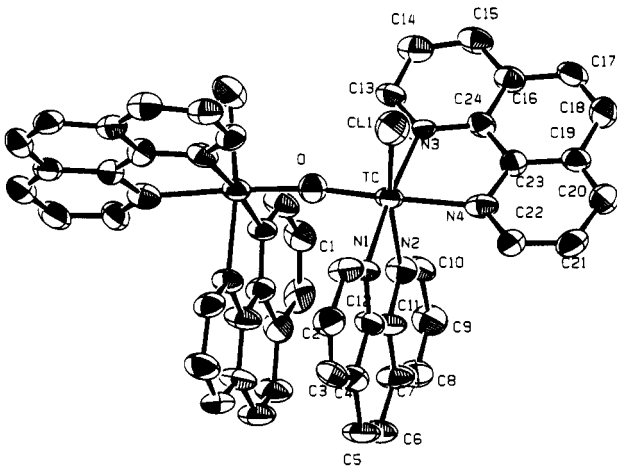

Figure 4. ORTEP diagram of $(\mu\text{-O})[Cl(phen)_2Tc]_2^{2+}$ with thermal ellipsoids at 30% probability.

molecules have co-crystallized by intercalation between the extended bipyridine ligands of the stacked complex ions. The halves of the free bipyridne are symmetry-related such that [C21–C24] overlaps substantially with [C12–C14] of a ligand bipyridine, and [C23, C24] overlaps with [C17, C18] on the other pyridine ring of the same, but symmetry-related, bipyridine ligand. In I, these distances are 3.50(7) and 3.45(9) Å, respectively. The other bipyridine ligands which are cis to the bridging oxygen interact and align with their symmetry related counterparts within the same molecule. The two pyridine rings in the bipyridine coordinated through N1 and N2 are canted by 6.91° and 4.90° in I and II, respectively. The two pyridine rings coordinated through N3 and N4 are canted by 9.21 and 7.75°, for I and II, respectively.

Comparison with the packing for $(\mu\text{-O})[Cl(phen)_2Tc]_2Cl_2\cdot 4H_2O$ illustrates a degree of isomorphism, but with two water molecules situated at the edges of the phenanthroline rings. These are hydrogen bonded together at an O1–O2 distance of 2.96(3) Å, and O1 and Cl2 are also linked by a hydrogen bond at a distance of 3.28 Å. The water molecule containing O2 is 3.39(3) Å from C2 and 3.31(3) Å from C3 on the phenanthroline stacked with its symmetry-related counterpart (within the complex) and 3.35(3) Å from C18 on the other phenanthroline ring.

In all three complexes, the 2-fold symmetry axis relating the halves of the molecule dictates identical stereo configurations on either side of the molecule and the centrosymmetric space group requires the two enantiomers (ΔΔ and ΛΛ) to exist in equal abundance. The slight bend along the Tc–O–Tc axis allows the symmetry-related aromatic rings coordinated through N1 and N2 on opposite sides of the same molecule to interact at an average

contact distance of ~3.47 Å. Average Tc–Tc distance for the three molecules is 3.64 ± 0.01 Å, and the average Tc–O–Tc bond angle is 172(1)°. Average bond distances in the technetium coordination sphere are as follows: Tc–O, 1.824(5) Å; Tc–N_{eq}, 2.11(2) Å; Tc–N_{ax}, 2.13$_5$(2) Å; Tc–Cl, 2.413(8) Å.

Discussion

While $(\mu\text{-O})[Cl(bpy)_2Tc]_2Cl_2$ can be obtained by heating bipyridine in a water/ethanol solution of $[Cl_3(py)_3Tc]$, which is available from $NH_4[TcO_4]$[20] or from the intermediate materials $K_2[TcCl_6]$ or $Cl_4(PPh_3)_2Tc$,[7] the starting material used here, $[(n\text{-}Bu)_4N][TcOX_4]$ (X = Cl or Br), is more easily prepared from $NH_4[TcO_4]$ and so, overall, provides for a more convenient and general synthesis of the μ-oxo complexes. Since the same complex is so readily formed by different syntheses, it appears to be of appreciable thermodynamically stability.

The coordinated halides are easily lost from the phenanthroline complex, yielding a purple complex in aqueous solution. The elemental analysis of the hexafluorophosphate salt of the aquated phenanthroline complex, its diamagnetism, and close correspondencies with the spectra of the halide complexes indicate a similar charge and structure, which is most consistent with hydroxide replacing the halides in water to yield $(\mu\text{-O})[(OH)(phen)_2Tc]_2^{2+}$. Close similarities between the aqueous solution spectra of all the (III–III) complexes suggest that all exist as $(\mu\text{-O})[(OH)L_2Tc]_2^{2+}$ in water. At pH below 3 and above 12, precipitation of these complexes begins to occur, suggesting the initiation of a change in protonation state. On the other hand, the maintenance of a constant reduction potential over a wide pH range indicates that the dominant species remaining in solution is $(\mu\text{-O})[(OH)L_2Tc]_2^{2+}$. At low pH, the reduction potential of molecular oxygen becomes sufficiently high to oxidize the purple $(\mu\text{-O})[(OH)(phen)_2Tc]_2^{2+}$ to the orange, mixed-valent (III–IV) complex; however, this process occurs only slowly in air. Since raising the pH reverses the process, the mixed-valent ion may be oxidizing impurities or H_2O_2 formed in the air oxidation between pH 2 and 7. While above pH 7 the mixed-valent species is thermodynamically able to oxidize water, rapid reversion to the purple form between pH 4 and 7 suggests that other species serve to reduce it. The (IV–IV) ion, which was not isolated or characterized, may form on oxidation of the (III–III) or (III–IV) ions by peroxide or nitrate in acidic solutions and is thermodynamically able to oxidize water at low pH.

Spectra. Assuming D_{4h} symmetry for a linear molecule, the metal d_{xz} and d_{yz} orbitals mix with the μ-oxo p_x and p_y to form an $e_u(\pi)$ and $e_u^*(\pi^*)$ set along with a pair of b_{2g} and b_{1u} nonbonding π-orbitals.[21] As the symmetry descends to C_{2v} the degeneracy of the various levels are lifted; however, the highest occupied levels remain nonbonding π in character while the lowest unoccupied are π^*.[22] Consequently, the lowest energy transition in this type of complex is often assigned as largely $d_{\pi nb} \rightarrow d_{\pi^*}$ in character.[7] IEHT calculations of the ammine analog of I (Figure S3) suggest that the d_π–p(O)–d_π (π^*), d_{xy}–p(Cl) (π^*), and d_π–d_π (nb) levels are relatively close in energy and that p(Cl) (π_b and π_{nb}) $\rightarrow$ d_π–p(O)–d_π (π^*) transitions occur in the 525 nm region. These calculations also suggest that transitions arising from d_π (π^*_{Cl} and π_{nb}) $\rightarrow$ $d_{x^2-y^2}$ (σ^*) and d_{z^2} (σ^*) account for the 320- and 290-nm bands, respectively. Since near-infrared bands occurring in the mixed-valent state tend to be termed "intervalence-charge-transfer" (IVCT) regardless of whether the metal ions are weakly or strongly coupled, the band at 959 nm in $(\mu\text{-O})[(OH)L_2Tc]_2^{3+}$ might be so assigned. The analogous transition in the isoelectronic ion $O[(OH)(bpy)_2Ru]_2^{3+}$,[23] has been attributed to a lower-energy $d_{\pi nb} \rightarrow d_{\pi^*}$ transition or to a transition between two similar $d_{\pi nb}$ orbitals, which are only partially occupied in the mixed-valent state. The IEHT calculations suggest that the mixed-valent complex should exhibit several charge transfer bands between 794 and 876 nm that are predominantly p(Cl) (π and π_{nb}) $\rightarrow$ d_{xy} (π^*-Cl and π_{nb}) in character, which may account for the distinct low-energy shoulder on the 959-nm band.

Structures. As is common in μ-oxo technetium complexes,[10] the Tc–O–Tc moieties are nearly linear and the average Tc–O_μ distance for the three technetium structures (1.824(5) Å) is intermediate between that observed for Tc—O[24] and Tc=O.[25,26] The average bond distance is consistent with a bond order of 1.7[27] indicating significant π-bonding between the technetium atoms and the oxygen involving the donation of electron pairs in the oxygen p_x and p_y orbitals of the oxygen to d_π orbitals on the metal ions. The near linearity and partial π-bonding make it improbable that the bridges involve μ-OH, which usually gives strongly bent complexes with M–O bond distances similar to those of single bonds.[28] The Tc–N and Tc–Cl bond distances are well within the range observed in a variety of other technetium complexes,[24–26] and in II there is a small trans-influence exerted on N4 by the μ-oxo group.

Steric hindrance forces the halide ligands to adopt a slightly staggered configuration and pushes the equatorial plane (defined by N1, N2, N3, and X) back from the Tc by an average of 0.178(6) Å in the three structures. The staggered arrangement and the substantial average distance (3.64(1) Å) between the two technetiums is very similar to that observed in $[Cl_2(pic)_3Tc\text{–}O\text{–}TcCl_3(pic)_2]$, and $[Cl(pic)_4Tc\text{–}O\text{–}Tc(pic)Cl_4]$ (where pic = 4-methylpyridine)[5] and precludes significant metal–metal bonding. In comparing the structures of $(\mu\text{-O})[Cl_2(bpy)_2Tc]Cl_2$ with and without[7] the bipyridine of intercalation, only the Tc–O–Tc bond angle is significantly different on a 2σ basis, with the complex being slightly more bent (by 3°), when the additional, intercalating bipyridine is present.

In comparison with the structure of $(\mu\text{-O})[(H_2O)(bpy)_2Ru^{III}]_2^{4+}$, which is the reduced form of the water oxidation catalyst, $(\mu\text{-O})[O(bpy)_2Ru^{V}]_2^{4+}$,[29] the difference in the d^4 electronic configuration for Tc^{III} versus the d^5 configuration for Ru^{III} plays a notable role. Having both d_π orbitals partially occupied allows Tc^{III} to accept substantially more π-electron density from the μ-oxo's p_x and p_y orbitals so that the average Tc–O_μ distance for the three technetium structures is 0.046 Å shorter than the corresponding distance in $(\mu\text{-O})[(H_2O)(bpy)_2Ru]_2^{4+}$. Since relatively more charge on the technetium ions is neutralized in this fashion, less σ-donation from the nitrogens is required with the result that the average Tc–N_{eq} bond distance is substantially (0.07 Å) longer than the 2.04(1) Å observed in $(\mu\text{-O})[(H_2O)(bpy)_2Ru^{III}]_2^{4+}$. A slightly smaller difference (0.04 Å) is seen between the average of the Tc–N_{ax} distances trans to the bridging oxygen and the corresponding distance in $(\mu\text{-O})[(H_2O)(bpy)_2Ru]_2^{4+}$ (2.089(4) Å).[29] The relatively greater π-bonding to the μ-O in both the *xz*- and *yz*-planes may also account for the lower average bend along the Tc–O–Tc axis, which is 6.6° less acute than the corresponding angle (165.4°) angle in the ruthenium dimer.[29]

In correcting for the difference between aqua and halide equatorial ligands between the two structures, the differences already noted are likely to be accentuated, since less π-electron density would be donated to the Tc from water than from either

(20) Lu, J.; Yamano, A.; Clarke, M. J. *Inorg. Chem.* **1990**, *29*, 3483–87.
(21) Dunitz, J. D.; Orgel, L. E. *J. Chem. Soc.* **1953**, 2594.
(22) Weaver, T. R.; Meyer, T. J.; Adeyemi, S. A.; Brown, G. M.; Eckberg, R. P.; Hatfield, W. E.; Johnson, E. C.; Murray, R. W.; Untereker, D. *J. Am. Chem. Soc.* **1975**, *97*, 3039–3048.
(23) Raven, S. J.; Meyer, T. J. *Inorg. Chem.* **1988**, *27*, 4478–4483.
(24) Bandoli, G.; Mazzi, U.; Roncari, E.; Deutsch, E. *Coord. Chem. Rev.* **1982**, *44*, 191–227.
(25) Kastner, M. E.; Fackler, P. H.; Clarke, M. J.; Deutsch, E. *Inorg. Chem.* **1984**, *23*, 4683–4688.
(26) Kastner, M. E.; Fackler, P. H.; Lindsay, M. J.; Clarke, M. J. *Inorg. Chim. Acta* **1985**, *109*, 39–49.
(27) Pauling, L. In *The Nature of the Chemical Bond*; Cornell University Press: Ithaca, NY, 1960; p 239.
(28) Libson, K.; Deutsch, E.; Barnett, B. L. *J. Am. Chem. Soc.* **1980**, *102*, 2477–2478.
(29) Gilbert, J. A.; Eggleston, D. S.; Murphy, W. R.; Geselowitz, D. A.; Gersten, S. W.; Hodgson, D. J.; Meyer, T. J. *J. Am. Chem. Soc.* **1985**, *107*, 3855–3864.

Table VII. Comproportionation Constants for $(\mu\text{-O})[X(L)_2Tc]_2^{2+}$

complex	K_{com} (10^{-10} M^{-1})	media
$(\mu\text{-O})[Cl(bpy)_2Tc]_2^{2+}$	20	0.1 M TEAP/CH_3CN
$(\mu\text{-O})[Br(bpy)_2Tc]_2^{2+}$	14	0.1 M TEAP/CH_3CN
$(\mu\text{-O})[Cl(phen)_2Tc]_2^{2+}$	17	0.1 M TEAP/CH_3CN
$(\mu\text{-O})[(OH)(phen)_2Tc]_2^{2+}$	3.1	0.1 M LiCl/H_2O

[a] Comproportionation is the reaction of a higher and lower oxidation state of the same complex to give an intermediate state. For compound I, this would be: $[I]^{4+} + [I]^{2+} \rightarrow 2\ [I]^{3+}$. $\ln (K_{com}) = F(E_1 - E_2)/RT$. The tendency for this reaction to occur indicates the degree of delocalization of the unpaired electron in the intermediate oxidation state.

halide. The greater ability of Tc^{III} over Ru^{III} to accept π-electron density from oxygen ligands is also reflected in the relative acidities of the two aqua complexes. $(\mu\text{-O})[(H_2O)(bpy)_2Ru]_2^{4+}$ has pK_a values of 5.9 and 8.3, while no change in protonation state for $(\mu\text{-O})[(HO)(phen)_2Tc]_2^{2+}$ was observed over a wide pH range. Consequently, the aqua ligands on the putative $(\mu\text{-O})[(H_2O)(bpy)_2Tc]_2^{4+}$ are probably much more acidic relative to the ruthenium case, reflecting a greater drainage of electron density from the aqua ligand onto the metal ion.

Electrochemistry. The ease with which halide ligands are lost from these complexes strongly suggests that the reduction potentials in aqueous solution (Table VI) are for the dihydroxo species, $(\mu\text{-O})[(HO)L_2Tc]_2^{2+}$. The electrochemical measurements indicate that these complexes can be oxidized or reduced in single-electron steps. While the redox processes corresponding to E_1 and E_2 were always reversible, at least on the relatively rapid voltammetric time scales employed, the situation for E_3 is more complicated. In acetonitrile, the E_3 reduction of $(\mu\text{-O})[(HO)(phen)_2Tc]_2^{2+}$ is pseudo-reversible in that only the first scan on a platinum electrode (Figure 2) yielded a reversible wave form. Following this, it is likely that the solvent coordinates as a result of reductively filling one of the d_π-orbitals, which should promote retrodative bonding to acetonitrile, or the complex dissociates due to a concomitant diminution in π-bonding to the μ-O. The wave form associated with E_3 then shifts negatively and becomes mixed with that for reduction of the ligand (truncated in Figure 2), to give a large, irreversible current peak. E_3 for the bipyridine complexes is resolved and reversible in aqueous media; however, in acetonitrile the reduction peak of this couple appears to overlap with the ligand reduction current, since a large irreversible reduction peak is seen, while an oxidation peak of approximately the same size and shape as those for E_1 and E_2 is evident.

The comproportionation constants (K_{Com}) listed in Table VII are so large as to indicate resonance sharing of the unpaired electron between the two Tc's in the mixed-valent system, i.e. the two centers are strongly coupled (Robin and Day class III),[30] and are more appropriately designated as (3.5–3.5) rather than (III–IV) dimers. The high K_{Com}'s also confirm the "symmetry-corrected" K_{Com}'s previously estimated for the asymmetric and dissymmetric μ-oxo complexes ($[X_2(py)_3Tc\text{–}O\text{–}TcX_3(py)_2]$ and $[X(py)_4Tc\text{–}O\text{–}Tc(py)X_4]$) as being in the range of 10^9–10^{10}.[5] In comparison with these complexes, the E_1 values reported here are about 0.6 V higher, while the E_2 values are 1.2 V higher. These differences are attributed to the three additional π-acceptor pyridine rings (and three fewer π-donor halides) in the present complexes. The symmetric nature of the complexes, which should enhance the resonance effect, and an additional small resonance enhancement owing to the coupling of the bipyridine rings should further stabilize the lower oxidation states. The summation of these effects readily explains why the present complexes are isolated in the lower (III–III) oxidation state, rather than as a mixed valent species. Reduction to the (II–III) state results in dissociation of the dinuclear ion, since the electron is added to a π^* orbital (Figure S2) and the electrostatic interactions stabilizing the μ-oxide are reduced.

(30) Robin, M. B.; Day, P. *Adv. Inorg. Chem. Radiochem.* **1967**, *10*, 247.

The high affinity of technetium for anionic oxygen ligands accounts for the deprotonation of the added aqua ligands to the hydroxo form. This contrasts with the analogous ruthenium system in which the dihydroxo form exists only above pH 8.[29] The pH-independent reduction potentials listed in Table VI are sufficiently high that the (IV–IV) ions are thermodynamically allowed to oxidize water to O_2 in four 1-electron steps and the (III–IV) ions can similarly oxidize water above pH 7. Nevertheless, since the first 1-electron oxidation to yield HO• lies at 2.85 V, these processes are not likely to proceed rapidly. This contrasts with the water oxidation system involving $(\mu\text{-O})[(H_2O)(bpy)_2Ru^{III}]_2^{4+}$, in which a 2-electron process merges with a 1-electron process below pH 3 to form a 3-electron process sufficiently positive to couple with a final 1-electron process to (in principle) yield a 4-electron potential sufficiently high to oxidize water.[29] Consequently, in the technetium system no multielectron process occurs and facile catalytic water oxidation was not observed. The reduction potential (E_2) for the process (IV-III) $\rightleftarrows$ (III–III) of $(\mu\text{-O})[(HO)(bpy)_2M]_2^{3+}$ is 0.37 V higher for Tc relative to Ru (0.44 V),[29] which suggests that the lower valent states of Tc are better π-donors to bipyridine ligands than similarly charged ruthenium ions. This is consistent with the relative potentials for $[(bpy)_3M]^{3+,2+}$, which are 2.2 V for Tc[7] and 1.5 V for Ru[31] in organic solvents.

While no attempt was made to elucidate the mechanism of nitrate (or peroxide) oxidation of $(\mu\text{-O})[(HO)(phen)_2Tc]_2^{2+}$, it is conceivable that this proceeds by O-atom transfer[32] to the technetium dinuclear complex to form NO_2^- (or H_2O in the case of peroxide) and a complex containing $O{=}Tc^{IV}\text{—}O\text{—}Tc^{IV}\text{—}OH$, which then reacts with a second molecule of the (III–III) ion to give the mixed-valent complex. Since the NO_3^-/HNO_2 couple (E° = 0.94 V) is in the range of the (III–III)/(III–IV) couple and is pH dependent, it is capable of driving the latter couple in either direction depending on the pH. Similarly the H_2O_2/H_2O couple (E° = 1.776 V) and the O_2/H_2O_2 couple (E° = 0.6824 V) are both pH dependent with the former easily oxidizing the (III–III) ion at low pH and the latter capable of reducing the (III–IV) ion as the pH increases.

Conclusion. Complexes of the type $(\mu\text{-O})[XL_2Tc]_2^{2+}$ (L = phen, bpy; X = Cl, Br, OH) are strongly coupled with the π-acceptor ligands stabilizing the $[Tc^{III}\text{–}Tc^{III}]$ oxidation state. The halide ligands are easily lost in aqueous media and the high affinity of Tc for anionic oxygen ligands accounts for the stabilization of the dihydroxy form over a wide pH range. Bonding to the bridging oxygen through π-bonding appears stronger in Tc^{III} than in Ru^{III}, which probably arises from d^4 versus d^5 electronic configurations. Comparison of reduction potentials indicates that Tc is a better π-donor to aromatic nitrogen heterocycles than Ru. While the corresponding one-electron reduction potentials for Tc are higher than for Ru, failure of these potentials to converge as a function of pH into a multielectron process precludes the facile oxidation of water.

Acknowledgment. This work was supported by NSF Grant CHE-8618011 and PHS Grant GM26390. We thank Dr. Mark Roe for crystallographic advice.

Supplementary Material Available: Figures showing an ORTEP diagram of $(\mu\text{-O})[Cl(bpy)_2Tc]_2^{2+}$ (Figure S1), a packing diagram for $(\mu\text{-O})[Br(bpy)_2Tc]Br_2\cdot bpy$ (Figure S2), and an IEHT MO energy level diagram (Figure S3) and tables giving the complete crystallographic data, H-atom positions, temperature factors for non-hydrogen atoms, bond distances and angles, and least-squares planes (32 pages). Ordering information is given on any current masthead page.

(31) Lever, A. B. P. *Inorg. Chem.* **1990**, *29*, 1271–1285.
(32) Craig, J. A.; Holm, R. H. *J. Am. Chem. Soc.* **1989**, *111*, 2111–2115.
(33) Johnson, C. K. *ORTEPII. Report ORNL-5138.*; Oak Ridge National Laboratory: Oak Ridge, TN, 1976.